Available online at www.sciencedirect.com
ScienceDirect
International Journal of Heat and Mass Transfer 51 (2008) 4367–4378
International Journal of HEAT and MASS TRANSFER
www.elsevier.com/locate/ijhmt

Rapid macromolecular synthesis in a microfluidic channel with an oscillating flap

Ruth A. Lambert [a], Siddhartha Das [b], Marc J. Madou [a], Suman Chakraborty [b], Roger H. Rangel [a,*]

[a] Department of Mechanical and Aerospace Engineering, University of California, Irvine, CA 92697-3975, USA
[b] Department of Mechanical Engineering, Indian Institute of Technology, Kharagpur 721302, India

Received 4 June 2007; received in revised form 30 November 2007
Available online 6 March 2008

Abstract

This study explores a method of enhancing the rates of macromolecular transport through a microchannel by introducing an oscillating mechanical flap in the fluidic system. A theoretical model is developed to determine the enhancement of macromolecular transport to a reaction site located along the channel surface. A numerical analysis is performed by considering a hinged flap located on the top or bottom walls of the channel. An order of magnitude analysis is conducted to estimate the reaction time which is bounded by the diffusion and the flow residence time. The period of oscillation is chosen to match the surface reaction time. The values of the characteristic flow variables adopted in this study, are representative of typical biomolecular transport processes confined to microscale geometries. With background flow, the results of the numerical analysis show that the mechanical actuator behaves like a miniature pump that drives a favorable gradient of macromolecules towards the surface reaction sites within an initial lapse of time. In a stagnant fluid, the results show that the moving flap behaves like a stirring agent bringing fluid with a higher concentration in contact with the reaction site and enhancing the surface concentration. In the latter case, the effect of the moving flap increases as the reaction progresses. The moving flap has the largest beneficial effect on surface concentration in the presence of a background flow when the position of the moving flap is along the top wall above the reaction site.

Keywords: Mechanical actuator; Oscillating micro-cantilever; Moving flap; Fast DNA hybridization; Microchannel flow; Mass transport

1. Introduction

A great interest in using microdevices to enhance biomolecular processes such as protein synthesis and DNA hybridization exists in the biomedical industry [1]. Early developments in this area of research focused on the detection of target molecules in a given sample using heterogeneous macromolecular assays. The assays contain probe molecules that are bound to a solid substrate. When a liquid sample is brought into contact with the macromolecular assay, the target molecules migrate towards the substrate by diffusion [2] and react with the probe molecules. Microarray technologies operating on such basic principles are typically said to be 'passive' in nature, since the underlying transport process strongly depends upon the diffusion of target molecules to the desired reaction sites.

Due to the dependence on diffusion, the 'passive' microdevices consume large amounts of biological samples, require long reaction times to produce detectable hybridization signals, and may provide results that cannot be replicated. In order to avoid these difficulties, many researchers have turned to alternative methods for biochemical analysis by exploring 'active' microfluidic systems. The advantages of the 'active' microdevices are they allow for the reactions to occur at the lowest possible sample concentrations, allow for shorter reaction times due

* Corresponding author. Tel.: +1 949 824 4033; fax: +1 949 824 8585.
E-mail address: rhrangel@uci.edu (R.H. Rangel).

0017-9310/$ - see front matter © 2008 Elsevier Ltd. All rights reserved.
doi:10.1016/j.ijheatmasstransfer.2007.11.053

Nomenclature

c	normalized bulk concentration
c_s	normalized surface concentration
C_w	bulk concentration in the liquid film near binding surface (M)
C_0	initial bulk concentration (M)
C_s	surface concentration of biomolecule (mol/m^2)
$C_{s,max}$	maximum surface concentration at reaction site (mol/m^2)
D	molecular diffusivity (m^2/s)
Da	Damkohler number, $C_{s,max}L_f k^1/D$
h	dimensionless channel height
H	channel height (m)
k^1	forward rate constant (1/M s)
k^{-1}	reverse rate constant (M)
l	dimensionless length
L	length (m)
n	inward facing unit normal
$\dot{m}''$	dimensionless mass transfer rate
$\dot{M}''$	mass transfer rate (mol/m^2 s)
Pe	Peclet number, UL_f/D
Re	Reynolds number, UL_f/v
t	dimensionless time
u	normalized velocity
U	velocity (m/s)
x	normalized horizontal direction parallel to channel bottom
y	normalized vertical direction

Greek symbols

ε	concentration ratio of biomolecule, $C_{s,max}/L_f C_0$
κ_A	equilibrium constant $k^1 C_0/k^{-1}$
v	kinematic viscosity (m^2/s)

Subscripts

c	characteristic value
ch	channel
d	diffusion
f	flap
0	initial or inlet value
r	residence (time)
sr	surface reaction
w	wall

Superscript

$'$	dimensional units

to enhanced mass transport, offer the ability to monitor several samples in parallel by using a multi-channel approach, reduce the potential for contamination by relying on an enclosed apparatus, and hold the overall promise for integration of several functions in a single apparatus. The advantages of the bio-microfluidic systems has led to the development of numerous protocols for 'macroscopic' handling of fluids and biological entities and are continuously being integrated on miniaturized chips for increased throughput, better automation, and reduced reagent consumption. Researchers have explored various actuating mechanisms to achieve faster rates of macromolecular transport through a microfluidic channel. In most cases, the convective transport has been externally induced through pressure driven flows [2], stagnation point flows over flat surfaces [3], or electroosmotically driven flows [4]. Each of these flow actuating methodologies, despite the intended elegance, has certain inherent constraints. Pressure driven flows, for example, might require large power inputs to achieve a substantial flow rate through a microconduit. Moreover, the pressure driven transport of biological molecules through a microchannel leads to other difficulties such as loss of injected samples due to dispersion and the inability to create complex flow patterns required for biotechnological applications [5]. A feasible alternative that is preferred by many researchers is the application of an external electric field to control transport and subsequent reactions of macromolecules. By employing electrokinetic flows, rapid transport of macromolecules in a microchannel is aided by virtually no gradients of flow velocities in the bulk [6]. The employment of stronger electric fields towards achieving faster rates of macromolecular transport, however, are significantly constrained by the possibilities of an uncontrolled rise in temperature due to Joule heating. The increase in bulk temperature of the medium is likely to disrupt the synthesis or hybridization process unless simultaneous cooling is implemented [6].

Since the actuation mechanisms commonly used in microfluidic devices present additional difficulties upon implementation, new alternatives that create local advection dominated areas and allow for spatio-temporal control are needed. To compensate for the difficulties encountered in pressure driven or electrical field driven flow, researchers have accordingly explored alternative local flow augmentation techniques such as channel-surface patterning [7,8], application of electric fields in different directions [7], and the creation of localized zeta potential gradients through surface reactions [9]. The implementation of these methodologies is limited by the practical constraints of achieving the desired geometry and chemical patterning through standard microfabrication techniques. An alternative flow augmentation mechanism with simple geometry is the employment of an oscillating surface in a microchannel which will enable a continuous supply of fluid with higher macromolecular concentrations close to the reaction sites.

The use of mechanical actuators or micro-cantilevers is not a new concept in the field of microfabrication for biological processes. Micro-mechanical actuators have been used as release valves, miniature pumps [10], and resonators for the detection and identification of biomolecules or chemical compounds [2,11]. Micro-cantilevers are also components in precision equipment such as the atomic force microscope which visualizes small scale phenomena including biomaterials [12]. Despite these advancements, the concept of an oscillating mechanical flap or actuator enhancing the rate of macromolecular reactions at a desired location in a microchannel has yet to be theoretically or numerically determined. Such actuators, however, are likely to increase the local advective transport in the vicinity of the reaction sites.

The objective of the present study is to investigate the idea of an oscillating flap as a mechanical actuator for faster macromolecular reactions in a microchannel. Since this configuration has not been explored previously, an accurate prediction of the mass and momentum transport characteristics is needed in order to optimize the design of the microfluidic system. A numerical model is developed to study the effects of the moving flap on the convective and diffusive mass transport of biomolecules toward a reaction site. The moving flap is a forced oscillator and is treated as a rigid solid body. Two separate cases are considered in order to identify the specific interaction mechanisms between the macromolecular transport and advective transport close to the moving flap. In the first case, the flap is designed to oscillate a stagnant fluid dispersed with the reactive agents. In the second case, a species-laden fluid enters through a small inlet located at the top of the enclosed microchannel and exits through a similar opening at the end of the channel as shown in Fig. 1. The location of the flap is arbitrary, however, in the present study the flap is positioned vertically at the channel midsection between the inlet and the outlet sections to avoid interaction with the recirculation zones at the channel entry and exit planes.

The characteristic variables used in the study are either the inlet velocity for background flow, U_0, the maximum flap velocity without background flow, U_f, the length of the flap, L_f, the flow residence time, L_f/U, the initial bulk concentration, C_0, and the maximum surface concentration, $C_{s,max}$. The characteristic stress is an inertial stress and is expressed as $\tau_c = \rho U^2$. An order of magnitude analysis, using typical values of the flow variables for biological processes is conducted. For the size of the microchannel considered, the value of the Reynolds number, $Re = UL_f/\nu$, is much less than unity, of the order 10^{-1}, and the Peclet number, $Pe = UL_f/D$, is of the order 10^4. The motion of the flap is oscillatory and the flap is free to move through a given angle or arc length at a specified frequency. The frequency of the flap motion in this study is chosen such that the period of oscillation, t_f, is identical to the reaction time t_{sr}. The reasons for the selection of the flap frequency is discussed further in Section 5. The inlet velocity, U_0, represents typical velocities encountered in microdevices and is chosen such that the flow Reynolds number, Re, and the Reynolds number of the flap, Re_f, are close in magnitude. The effect of the flap motion on the removal rate of the biomolecules from the bulk fluid is quantified by the total mass flow rate toward the wall, $\dot{m}_w$, and the surface concentration accumulated along the reaction site in time and space, c_s.

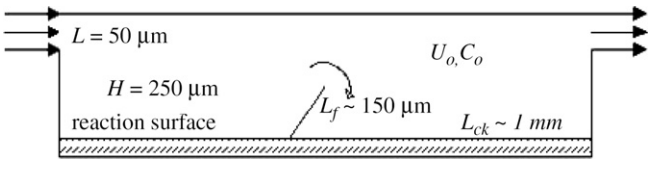

Fig. 1. Microchannel arrangement.

2. Mathematical formulation

2.1. Governing equations

The flow field is solved numerically in two dimensions, using the Navier–Stokes equations. The governing equations are written in non-dimensional form. The continuity equation is expressed as

$$\frac{\partial u}{\partial x} + \frac{\partial v}{\partial y} = 0. \tag{1}$$

The unsteady momentum equation in dimensionless form is expressed as

$$\frac{\partial \boldsymbol{u}}{\partial t} + (\boldsymbol{u}\cdot\nabla)\boldsymbol{u} = -\nabla p + \frac{1}{Re}\nabla^2\boldsymbol{u} \tag{2}$$

and the mass transport equation for the normalized concentration, c, is expressed as

$$\frac{\partial c}{\partial t} + \nabla\cdot(\boldsymbol{u}c) = \frac{1}{Pe}\nabla^2 c. \tag{3}$$

2.2. Surface reaction

In an operational microdevice, multiple biomolecular reaction or synthesis sites are positioned along the channel boundaries and have typical surface areas of order 10^2 μm^2 [13]. In this study, the entire bottom surface of the microchannel is treated as a reaction site in order to identify the specific location along the microchannel surface at which the biomolecular accumulation rate reaches a maximum. An order of magnitude analysis, considering the characteristic times of the process, is conducted in order to identify whether the moving flap will enhance the biomolecular adsorption rate towards the bottom surface, expressed in terms of c_s, and the total mass flow rate towards the wall, $\dot{m}_w$. The numerical results with the moving flap are compared to the flow conditions in the microchannel without the flap.

Intermolecular reactions that occur in the bulk fluid are treated as source terms in the governing mass transport

equation and have units of mol/m^3 s. Surface reactions, however, have units of mol/m^2 s and are generally accounted for through a flux boundary condition. The reaction or synthesis of a biomolecule along a surface can be described by a second-order rate equation with both a forward and reverse reaction rate [2,13,14]. The general rate equation for this type of process is well known and is described as

$$\frac{\partial C_s}{\partial t'} = k^1 C_w (C_{s,max} - C_s) - k^{-1} C_s, \tag{4}$$

where C_s is the surface concentration of the biomolecule, C_w is the bulk fluid concentration in the film near the wall, $C_{s,max}$ is the concentration of the probe molecules along the surface, and k^1 and k^{-1} are the forward and reverse rate constants, respectively. Since the channel walls are impermeable, the velocity at the wall is governed by the no-slip condition and the species flux toward the wall is purely diffusive. The boundary condition for the mass transport equation along the reaction surface is implemented through the relationship between the mass flux and the surface reaction:

$$\dot{M}''_w = -\frac{\partial C_s}{\partial t'}, \tag{5}$$

where the $\dot{M}''_w$ is the mass flux normal to the surface. Eq. (5) thus reduces to

$$n \cdot D \frac{\partial C}{\partial y'} = -\frac{\partial C_s}{\partial t'}, \tag{6}$$

where n is the inward unit normal vector at the bottom surface of the microchannel.

2.3. Scaling in a microchannel

The three time scales for bulk fluid flow near a reaction surface are the flow residence time, $t_r = L_f/U$, the time for synthesis or reaction time, $t_{sr} = L_f/C_{s,max}k^1$, and the diffusion time, $t_d = L_f^2/D$. For fluid motion generated by the moving flap in the given microchannel dimensions, the residence time is of order 10^{-2} s, the diffusion time is of order 10^2 s, and the time of reaction can vary between the two time scales depending on the biochemical process, as dictated by the value of the reaction rate, k^1. For the typical sets of parameters considered in this study, the reaction time is constrained between the residence and diffusion time, $t_r < t_{sr} < t_d$. Since the fluid residence time is the smallest of the three, it is used as the characteristic time, t_c, in the mathematical analysis.

When the rate equation (4) and flux boundary condition in Eq. (6) are expressed in dimensionless form, seven flow variables appear. Using dimensional analysis, this number can be reduced from seven to four dimensionless variables. The number of independent variables is consistent with the scaling of the reaction rate equations reported in the other studies [2,13]. The dimensionless variables that appear in Eqs. (4) and (6) are identified as the Damkohler number, $Da = C_{s,max}L_f k^1/D$, the equilibrium constant, $\kappa_A = k^1 C_0/k^{-1}$, the Peclet number, Pe, and the surface to bulk concentration ratio, $\varepsilon = C_{s,max}/L_f C_0$. In its dimensionless form, the rate equation can be expressed as

$$\frac{\partial c_s}{\partial t} = \frac{Da}{\varepsilon Pe \kappa_A}(\kappa_A c_w (1 - c_s) - c_s), \tag{7}$$

while the mass flux boundary condition at the reaction surface is expressed as

$$\left.\frac{\partial c}{\partial y}\right|_{y=0} = \varepsilon Pe \frac{\partial c_s}{\partial t}. \tag{8}$$

3. Numerical method

The flow field is solved using a pressure correction algorithm, which ensures a continuity satisfying pressure field upon convergence. An intermediate velocity field, $\boldsymbol{u}^*$, is calculated using an initial pressure field, p^n, in the following form:

$$\frac{d\boldsymbol{u}^*}{dt} = \boldsymbol{F}^n - \nabla p^n, \tag{9}$$

where $\boldsymbol{F}^n$ are the convection and viscous diffusion terms. The pressure difference, $\delta p = p^{n+1} - p^n$, is calculated by combining the expression $\boldsymbol{u}^{n+1} = \boldsymbol{u}^* - \nabla \delta p$ and the continuity equation (1) in the form of a Poisson equation, as follows:

$$\nabla^2 \delta p = \frac{\partial \nabla \cdot \boldsymbol{u}^*}{\partial t}. \tag{10}$$

Upon convergence, the pressure field at the current time step is calculated as

$$p^{n+1} = p^n + \delta p. \tag{11}$$

An updated velocity field is calculated using the new values for p^{n+1} in Eq. (11), until the desired level of convergence in the Poisson and continuity equations is obtained.

3.1. Representation of the moving flap

The position of the moving flap is identified using a distance function, ϕ, commonly used in the level set method [15]. Initially, the flap is in a vertical position and the expression for the initial distance function is $\phi_0 = -(x - x_0)$. The motion of the flap is modeled using the convection equation and known values for the velocity at the flap interface:

$$\frac{\partial \phi}{\partial t} + \boldsymbol{u} \cdot \nabla \phi = 0. \tag{12}$$

In this study the flap is a forced oscillator with a prescribed angular velocity of $\omega = A\sin(\beta t)$. The amplitude of oscillation is expressed as $A = \pi S/2r\,\Delta t$ where S is the arc length, r is the flap radius, and Δt is 1/2 the period of oscillation. The frequency of the flap motion is $\beta = \pi/\Delta t$. The velocity of the flap is thus $\boldsymbol{u} = \omega \times r$. The flap motion starts from an

initial vertical position and rotates in a clockwise direction towards the wall. The arc length, S, and the period of oscillation, $2\Delta t$, are variable parameters which are specified in the numerical analysis.

3.2. Boundary conditions

The boundary conditions for the governing equations are provided in Table 1. For the momentum equations, the no-slip boundary condition is implemented on the solid surfaces. In order to implement the no-slip condition on the moving flap, the flap is designated a small finite thickness of $\tau = 0.05$ or 1/2 the grid spacing. In order to solve the governing equations in finite-difference form on nodes bordering the flap, linear interpolation using the distance function, ϕ, and the known velocity of the moving flap is used to represent the ghost nodes that lie on the opposite side of the flap. For the case with background microchannel flow, the boundary conditions are the fully developed parabolic velocity profile at the inlet:

$$u = \frac{U}{U_m} = -6\left(\frac{y^2}{h^2} - \frac{y}{h}\right) \quad \text{at } x = 0 \tag{13}$$

and plug flow at the channel outlet

$$u = 1 \quad \text{at } x = l_{ch}, \tag{14}$$

thereby maintaining a constant flow rate through the device. For the case without background flow, the initial velocity is zero, $\boldsymbol{u} = 0$, throughout the flow domain and the no-slip condition is maintained on all four channel walls.

In the solution of the pressure correction equation (10), the intermediate normal pressure gradient $d\delta p/dn = 0$ is implemented along the solid walls and along the flap. Linear interpolation using the distance function ϕ is used to express ghost nodes that appear in the finite-difference equations bordering the flap interface. In the post calculation of the pressure field, p^{n+1}, the Neumann boundary condition derived from the momentum equation (2) is implemented to insure the correct flow behavior near the solid surfaces.

The boundary conditions for the mass transport equation are a uniform inlet concentration, $c = 1$, and zero initial concentration in the microchannel $c(t = 0) = 0$ for the case with background flow. For the stagnant case, the fluid filling the domain is at the initial concentration, $c(t = 0) = 1$. In the solution of the mass transport equation, zero concentration flux is maintained along the moving flap and along the solid walls. Linear interpolation is used for ghost nodes that appear in the finite-difference equations bordering the flap interface. In the model, the reaction kinetics are implemented along the entire bottom surface in order to identify ideal probe locations in which the moving flap will have the greatest influence.

4. Numerical validation

Time step and grid size independence tests were conducted to test the validity of the numerical code. To save computational time, the length of the microchannel was reduced to half of the length, $x = 3.3$, used in the study. A diagram of the variable spaced mesh is shown in Fig. 2 for a half channel. The tests were conducted for the moving flap problem with and without background channel flow in order to choose the optimal time and grid spacing for the final simulations in the full channel length, $x = 6.7$.

The optimal time step was chosen considering computational efficiency and differences in the results of less than 2% in comparison to the next lowest time step. Using a 101×51 mesh with an average grid spacing of $\Delta x = 0.03$, the numerical residuals and change in the flow variables are examined for four different time steps, $\Delta t = 0.01$, 0.005, 0.0025, and 0.002. The moving flap was positioned on the bottom channel surface at $x = 1.3$ in a microchannel with half the desired length, $x = 3.3$, to save on computational time. The case of background fluid flow is considered. The surface reaction boundary condition is implemented using typical values for biological processes given in Table 2. The angle of rotation of the moving flap was 80° and the frequency of the flap was 0.13 Hz. The percent difference in the values of the flow variables, $|u|$, c, and p are determined in each case by taking the summation of the percent difference with the results for the next lowest time step and dividing by the total number of nodes. The ideal time step for the average grid spacing of $\Delta x = 0.03$ is $\Delta t = 0.005$ with a percent difference in the calculation of the flow variables with the results for the next lowest time step of 1% for $|u|$, 0.4% for p and 1.1% for c. An error of approximately 1% is considered adequate for the purposes of the numerical model. At the chosen time step of 0.005, the numerical errors determined by the residuals of the governing equations are 2.7×10^{-2} for the momentum equations, 2.14×10^{-1} for the pressure field, and 3.89×10^{-7} for the mass transport equation.

The grid sized independence tests are conducted considering flap motion on the bottom channel surface for both

Table 1
Boundary conditions

Equation	Solid wall	Flap	Inlet/outlet
Momentum (2)	No slip	$\boldsymbol{u} = \omega \times \boldsymbol{r}$	$u = -6(\frac{y^2}{h^2} - \frac{y}{h}), u = 1$
Pressure (10)	$d\delta p/dn = 0$	$d\delta p/dn = 0$	$\delta p = 0$
Mass transport (3)	$dc/dn = 0$	$dc/dn = 0$	$c = 1$, $dc/dn = 0$
Surface reaction (8)	$\dot{m}''_w = -dc_s/dt$		
Pressure field	$Re\, dp^{n+1}/dn = f(u^{n+1}, v^{n+1})$		

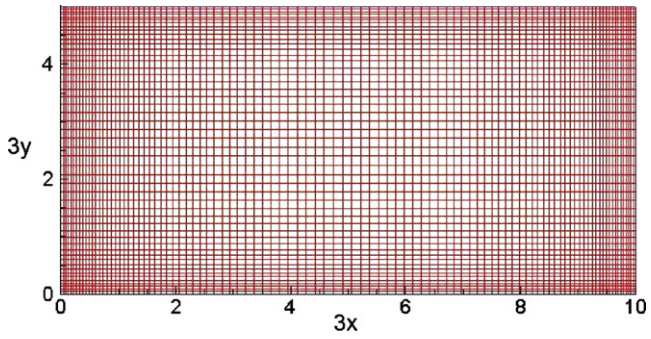

Fig. 2. Variable grid used in the numerical validation.

Table 2
Typical values of the flow variables encountered in biomolecular processes

Variable	Value[a]	Units	Variable	Value	Units
C_s	2×10^{-9}	mol/m^2	Re	0.22	
C_0	1×10^{-6}	M	Re_f	0.045	
k^1	1×10^{4}	(M s)$^{-1}$	Pe	1999	
k^{-1}	0.01	s^{-1}	Pe_f	400	
D	1×10^{-10}	m^2/s	Da	30	
v	9×10^{-7}	m^2/s	ε	13.3	
L_i	50	μm	κ_A	1	
L_f	150	μm	t_d	225	s
f	0.13	Hz	t_r	0.11	s
U_0	1.33	mm/s	t_{sr}	7.5	s
U_f	0.27	mm/s	t_f	7.5	s

[a] Gervais and Jensen [2], Pappaert and Desmet [13].

background fluid flow and zero background flow. A grid size independence test is conducted using four different grid sizes with an average grid size spacing of $\Delta x = 0.03$, 0.022, 0.017, and 0.013 using a constant grid spacing to time step ratio, $\Delta x/\Delta t = 20$ for the case with flow, and $\Delta x/\Delta t = 50$ for the case with zero background flow. The values of the flow variables used in the numerical trials are shown in Table 2 for a constant flap frequency of 0.13 Hz. The Reynolds number for the case with background flow is based upon the inlet velocity and is equal to 0.22 while the Reynolds number for the case with no background flow is based upon the maximum flap velocity and is equal to 0.045.

The performance of the numerical code for the different grid spacing is evaluated by comparing the numerical residuals and the percent difference in the average surface and wall concentrations at a given time. The average percent difference in the concentration values on a particular grid is determined by taking the summation of the percent difference in the values from the grid with the next smallest grid spacing and dividing by the total number of grid points along the wall. The values of the residuals and the difference in the surface and bulk fluid wall concentrations are shown in Table 3 for the case of flap motion with and without background fluid flow. A plot of the surface wall concentration showing the results for each grid is shown in Fig. 3 for the case of background flow and zero background flow. The results show that with decreasing grid size, the numerical code converges to a solution. The grid with dimensions 151×76 with an average grid spacing of $\Delta x = 0.022$ is chosen as the ideal grid size for the numerical simulation since the percent difference for c_s and c_w with

Table 3
Numerical results of grid size independence test

Grid	Numerical residuals			% Δc_s
	$\|u\|$	p	c	
With flow t = 300				
101×51	2.67×10^{-2}	2.14×10^{-1}	3.89×10^{-7}	4.8
151×76	4.05×10^{-2}	3.36×10^{-1}	2.40×10^{-7}	0.98
201×101	6.66×10^{-2}	4.95×10^{-1}	2.05×10^{-7}	2.1
251×126	1.62×10^{-1}	8.88×10^{-1}	2.27×10^{-7}	–
No background flow t = 60				
101×51	2.61×10^{-1}	1.57	1.38×10^{-7}	2.6
151×76	4.35×10^{-1}	2.45	7.79×10^{-8}	1.81
201×101	6.26×10^{-1}	3.44	8.46×10^{-8}	2.6
251×126	1.81	6.12	8.60×10^{-7}	–

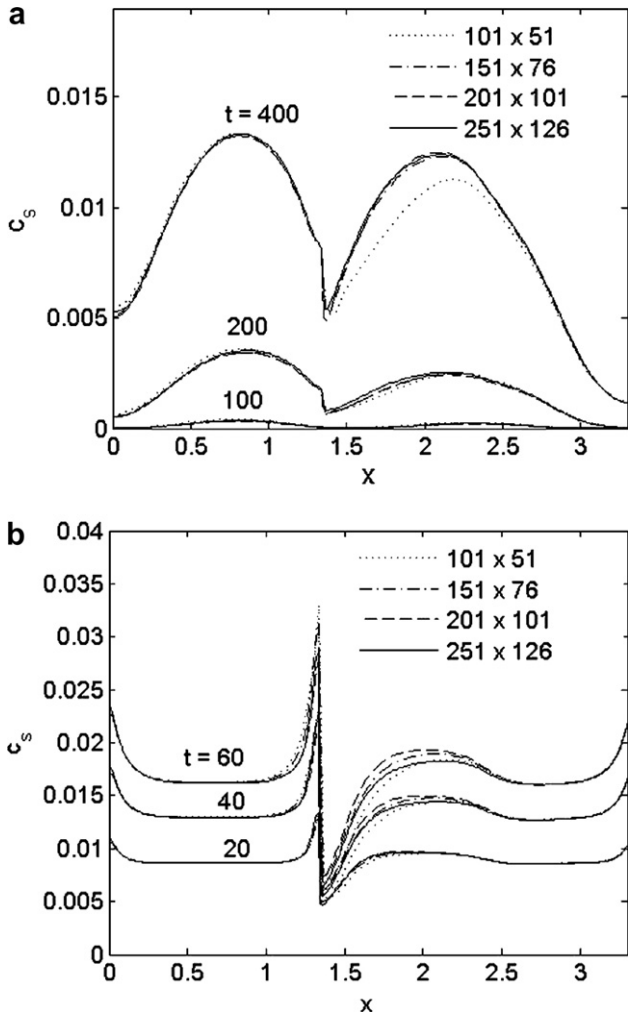

Fig. 3. Surface wall concentration profiles along channel bottom for flap motion (a) with background flow and (b) without background flow for $f = 0.13$ Hz and a total simulation time of $t' = 56.4$ s.

the next smallest grid was less than 2% both background flow conditions. The average numerical residuals for this grid size are 4×10^{-2} for the momentum equation, 2×10^{-1} for the Poisson equation, and 4×10^{-7} for the mass transport equation for the case of fluid flow as shown in Table 3.

5. Results and discussion

The relationship between the characteristic variables and the equilibrium surface concentration, $[c_s]_e$, can be found by finding the maximum of Eq. (7) using a time average film or wall concentration, $c_{f,avg}$. The equilibrium surface concentration is governed by the equilibrium constant, κ_A, and is expressed as

$$[c_s]_e = \frac{c_{f,avg}}{c_{f,avg} + 1/\kappa_A}. \quad (15)$$

The variation of the equilibrium concentration, with average film concentration, is shown in Fig. 4 for different values of the equilibrium constant κ_A. For fixed κ_A and small $c_{f,avg}$, equilibrium is attained at a lower value of the surface concentration implying that even at the equilibrium condition a large number of probe sites remain unreacted. In this lower range, even a slight increase in the average film concentration forces the equilibrium reaction, as shown in Eq. (7) with the LHS equated to zero, towards the right and increases the value of equilibrium surface concentration. For larger values of, implying larger values of $[c_s]_e$, the backward reaction governing the dissociation of the reacted targets, as shown in the second term in the RHS of Eq. (7), becomes equally important so that the equilibrium value of surface concentration remains virtually unaltered. Analogous to the effect of $c_{f,avg}$, the effect of the variation of κ_A on is found to be more prominent at relatively smaller values of κ_A, because of the fact that for such values of κ_A, remains relatively small. This allows the forward reaction, as shown in the first term in the RHS of Eq. (7), to occur at a larger extent resulting in a larger change in the value of $[c_s]_e$.

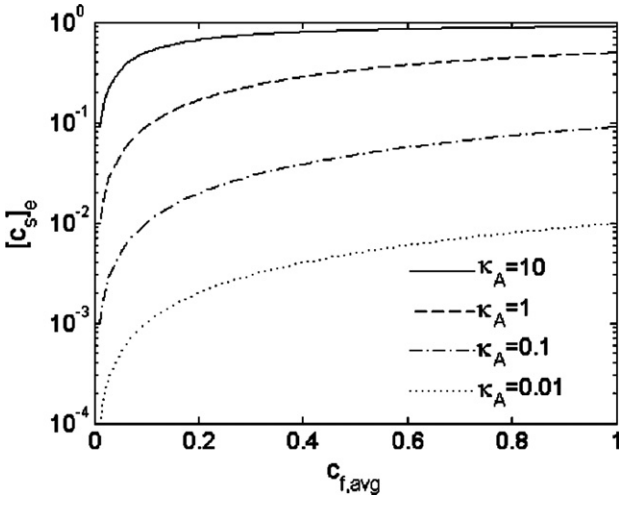

Fig. 4. Equilibrium surface concentration versus time average film concentration for $\kappa_A = 0.01$–10.

The typical input parameters used in the numerical analysis are listed in Table 2. The Reynolds number is calculated using a viscosity of the bulk fluid identical to that of water. A general diffusivity for a given biomolecule in water is of the order $D = 10^{-10}$ m^2/s and is used in this study. A frequency of $f = 0.13$ Hz and a sweep angle of 80° is considered such that the maximum flap velocity is equivalent to approximately 20% the inlet velocity, U_0. At this frequency, the period of oscillation is identical to the reaction time, $t_f = t_{sr}$. Imposition of such equality has strong physical implications. If the oscillations of the flap are much faster than the reaction time, $t_f < t_{sr}$, the biomolecules that have been brought close to the reaction sites by the oscillatory flap motion do not get the sufficient time to react and are driven away from the reaction sites during the reverse motion of the flap. On the other hand, if the flap oscillations are much slower than the reaction time, $t_f > t_{sr}$, the rate of supply of biomolecules at the reaction sites is too low to be of any perceptible consequence. A total simulation time of $t' = 56.3$ s for 7.5 oscillations of the moving flap is used in the numerical model. This time is less than the saturation time for the given variables.

In order to locate potential surface reaction sites along the bottom channel wall, the entire surface is treated as a reaction site in order to identify the regions in which the moving flap enhances the biomolecular reaction. The effect of the flap motion on the amount of species removed from the bulk fluid is determined for two locations of the moving flap, the first position along the bottom channel wall and the second position along the top of the channel wall. In both cases, the flap is located at a position that is 40% of the channel length, at $x = 2.67$, in order to avoid the effects of the flow inlet and outlet. The flap effect on saturation time and the species removal rate is analyzed by looking at the time development of the surface concentration, the total mass flow rate toward the wall, and the surface concentration profile along the wall. The cases with and without background flow are considered.

5.1. Flap motion with background flow

A diagram of the concentration contours for the moving flap at $t = 460$ with background flow is shown in Fig. 5, for a flap frequency of 0.13 Hz. Initially, the fluid in the domain has a concentration of zero. At the elapsed time, the flap lies at a 30° angle moving in a clockwise direction for the flap at the top surface, and a counter-clockwise direction for the flap at the bottom surface. For the given parameters in Table 2, this is equivalent to $t' = 51.8$ and 6.8 flap oscillations.

The variation of the surface concentration along the wall at different times is shown in Fig. 6 with and without the moving flap. The enhancement in the reaction rate is characterized by a larger value of the surface concentration, c_s.

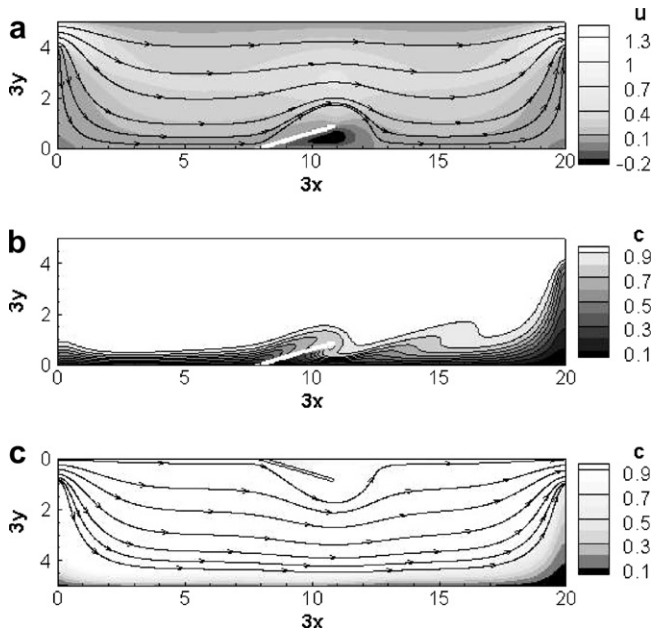

Fig. 5. Results for flap motion with background flow showing (a) velocity contours and streamlines for flap on bottom surface; (b) concentration contours for flap on bottom surface and (c) concentration contours and streamlines for flap on top surface using base values in Table 2.

The times shown in the figure are less than the saturation time, the time at which the surface concentration has reached the final equilibrium value. For the flap located at the top wall, the results in Fig. 6a show that the flap enhances the reaction rate at locations along the wall both to the left and to the right of the moving flap. The degree of enhancement is reduced farther from the flap. The flap at the top wall "pushes" the fluid containing the macromolecules and forces them closer to the reaction site at the bottom channel wall. This push is strongest directly below the flap and operates in conjunction with the convective supply of biomolecules in the background flow. The maximum effect is approximately one-third the characteristic length, L_f, to the right of the flap at $x = 3$ along the bottom wall. When the flap is located along the bottom wall, it is apparent from Fig. 6b that the flap enhances the species removal rate at a distance of $1.3L_f$ to the right of the flap at $x = 4$. At locations along the wall closest to the moving flap, the plots in Fig. 6b show that the depletion rate is significantly reduced as indicated by a steep reduction in the value of the surface concentration, c_s. This reduction in surface concentration can be attributed to the fact that at such locations the flap "squeezes" the flow. This squeeze motion drives the fluid containing the biomolecules away from the reactive surface and reduces the reaction rate.

The total mass flow rate toward the wall, $\dot{m}_w$, is shown in Fig. 7 and is calculated as follows:

$$\dot{m}_w = \int_0^{l_c} \left.\frac{\partial c}{\partial y}\right|_{y=0} dx. \tag{16}$$

The results show that the flap enhances the total mass flow rate towards the wall and that the increase in the mass flow

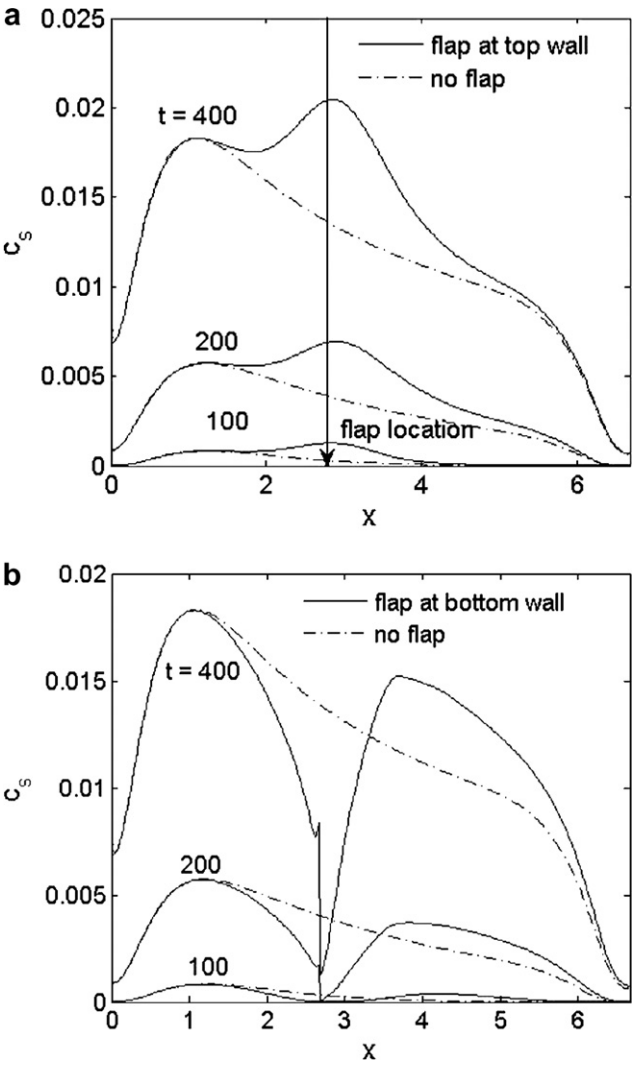

Fig. 6. Surface concentration along the bottom channel wall at different times for a flap location (a) along the top wall and (b) along the bottom channel wall at $x = 2.67$ for the case with background flow.

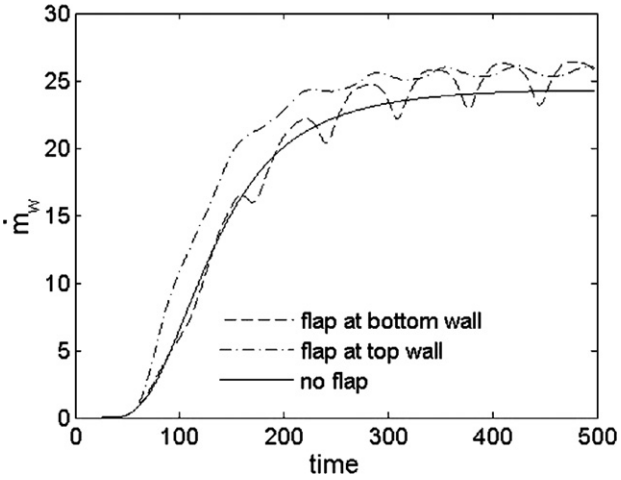

Fig. 7. Total mass flow rate at the bottom channel surface with and without flap motion.

rate is greatest at the initial time period when the flap is located on the top channel surface. The magnitude of the mass flow rate varies depending upon the position of the flap and this fluctuation is most pronounced when the moving flap is located on the bottom channel surface. For the case of the moving flap on the bottom surface, the maximum flow rate occurs when the flap is sweeping in a counterclockwise direction. Initially the mass flow rate is less than the case with the flap on the top wall, however, as time progresses the difference diminishes and the quasi-steady value is the same. The quasi-steady value for both flap arrangements at $t = 500$ is approximately 8% higher than the value for the case without the moving flap.

The effect of the increase in mass flow rate toward the wall on the surface concentration is shown in Fig. 8. The time development of the surface concentration is shown at the locations in which the moving flap has the greatest positive effect on the species removal from the bulk fluid as shown in Fig. 6. The percent difference in the surface wall concentration with and without the moving flap is shown in Fig. 9. At $t = 500$, the percent difference in the surface concentration with and without the moving flap is 51% for the case with the flap location on the top wall and 37% for the case with the flap on the bottom wall. At this time, the flap has undergone 7.5 oscillations. The results show that the effect of the flap in terms of percent difference in surface wall concentration actually decreases as time progresses, indicating that the flap behaves both like a pump and stirring agent, moving the entering concentration plume toward the reaction zone and continuing to bring fluid with higher concentrations in contact with the surface reaction site. The effect of the flap is greatest during the initial time period after which time the percent increase reaches a quasi-steady value.

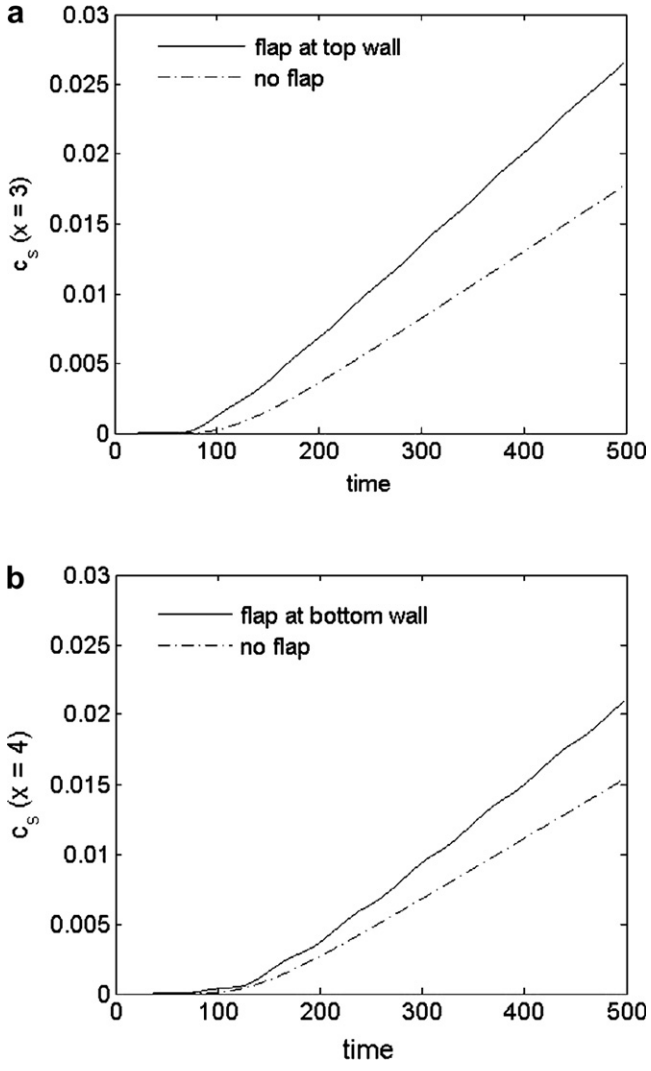

Fig. 8. Time development of the surface concentration for flap motion in background flow at (a) $x = 3$ for moving flap at top wall and (b) $x = 4$ for moving flap at bottom wall.

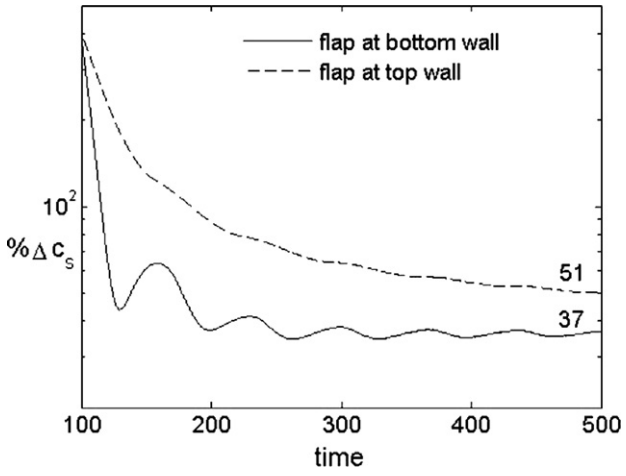

Fig. 9. Percent difference in the surface concentration for the case with and without the moving flap in background flow.

5.2. Flap motion in a stagnant fluid

The effect of a moving flap on enhancing the surface reaction at the bottom wall in a stagnant fluid, is considered for

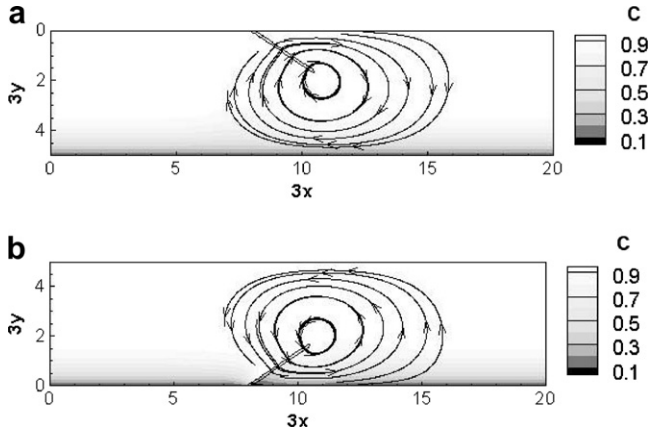

Fig. 10. Concentration contours and streamlines for flap motion in a stagnant fluid for a flap located on the (a) top wall and (b) bottom wall using typical values in Table 2.

a flap location on either the top or bottom surfaces. A contour plot of the concentration field and the streamlines due to the flow generated by the moving flap are shown in Fig. 10 at time $t = 57.5$. At $t = 0$, the initial concentration in the bounded domain is $c = 1$ and the concentration boundary layer begins to develop along the bottom surface, where the reaction occurs. The concentration boundary layer is visible in Fig. 10 along the bottom channel wall. Using the values in Table 2, the total elapsed time is $t' = 32.4$ s and the flap has oscillated 4.3 times. At this time, the flap on the top wall is moving counterclockwise and the flap on the bottom wall is moving in a clockwise direction.

The surface wall concentration along the bottom channel surface is shown in Fig. 11 at different times with and without flap motion. When the flap is located on the bottom wall, the motion of the flap enhances the surface wall concentration to the right of the flap and to the left of the flap at the flap base. Fig. 11b shows that with the flap located at the channel bottom wall, the concentration contours spread out towards the right of the flap, whereas they are confined to only a restricted zone of influence to the left of the flap. Thus, towards the left of the flap, the maximum enhancement in concentration occurs at the base of the flap in the shape of a sharp peak, which subsequently undergoes a rapid spatial decay. On contrary towards the right of the flap, the enhancement in surface concentration due to flap motion is spread over a larger distance, with a peak in surface concentration occurring at $x = 3.3$, a distance of $2/3L_f$. It is also worth mentioning here that the positive effects of flap oscillation do not extend significantly along the bottom surface and remain virtually confined around this point within an area as large as $1/3L_f$. This is in sharp contrast with the results for the case with the background flow, where the enhancement due to the flap motion extends along the entire bottom surface to the right of the flap as shown in Fig. 6b. The presence of the flow field ensures that the additional supply of the macromolecules due to the flap motion is not only confined to the regions close to the flap but are transmitted to locations downstream, thereby exhibiting an enhancement in the c_s value even at locations further away from the flap. For the flap motion at the top wall, the positive influence of the moving flap on the surface wall concentration is barely visible in the figure. The maximum increase in the surface concentration for this configuration is 3.17, a distance of $1/2L_f$ to the right of the flap. When there is a background flow, it ensures that the local pumping effects induced by the flap motion at the top wall maintain a continuous supply of macromolecules for subsequent transmittal towards the bottom wall, thereby enhancing the values of c_s as shown in Fig. 6a. Without background flow, however, this local pumping remains weak so that at locations further away from the flap, near the reactive channel bottom wall, the concentration flux of the macromolecules due to the flap motion becomes comparable to the diffusive transport so that there is virtually no augmentation in the value of c_s, as shown in Fig. 11a. The results show that for flap motion in a stagnant and bounded fluid, the largest increase in the accumulation of the biomolecules along the bottom wall occurs when the flap is located on the bottom surface.

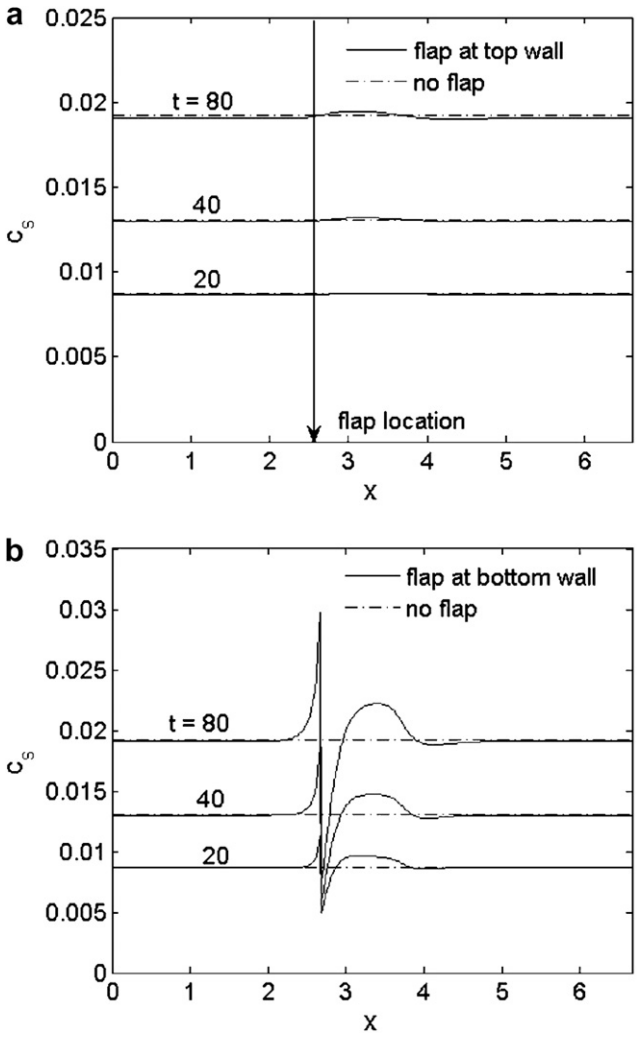

Fig. 11. Surface concentration along the bottom channel wall at different times for a flap location (a) along the top wall and (b) along the bottom channel wall at $x = 2.67$ for flap motion in a stagnant fluid.

The net mass flow rate for the cases with and without the moving flap and the time development of the surface concentration at $x = 3.3$ is depicted in Fig. 12. The point of greatest enhancement in the surface wall concentration is clearly seen to be located towards the right of the flap. The point to the left of the moving flap is not analyzed further since it represents a sharp peak in surface concentration at the base of the flap and does not extend any further along the bottom surface, making it a difficult location to place a probe. The results show that the moving flap does not enhance the overall mass flow rate towards the wall, and that the increase in surface concentration is a consequence of the redistribution of the solute close to the substrate wall. A plot of the surface wall concentration in Fig. 12b shows that the difference in the surface wall concentration between the case with and without the

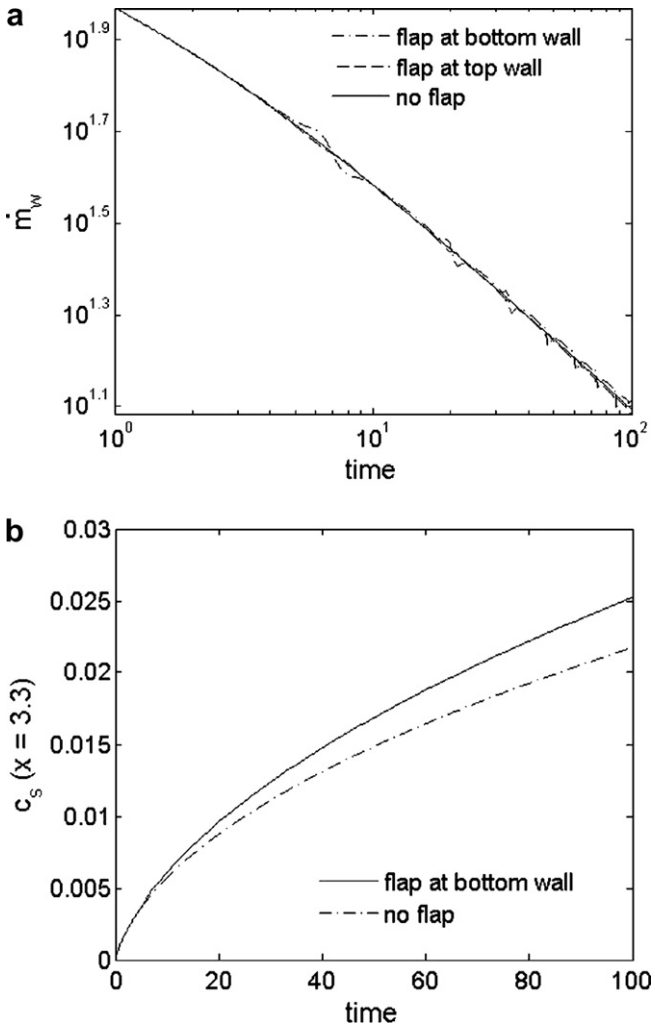

Fig. 12. Effect of moving flap in a stagnant fluid on the time development of (a) the total mass flow rate and (b) the surface wall concentration at $x = 3.3$.

moving flap at the location where the moving flap has the greatest influence at $x = 3.3$ continues to increase in the time interval shown, with a maximum percent increase of 16.3% at $t = 100$. At this time, 56.3 s have elapsed and the flap has oscillated 7.5 times. In a stagnant fluid, the moving flap behaves as a stirring agent bringing the fluid with higher concentrations in contact with the wall. Unlike the case of a moving flap in background flow with an initial concentration of $c = 0$, in a stagnant fluid the moving flap has the greatest effect as time increases when and the overall concentration in the microchannel is depleted.

6. Conclusions

The role of mechanical mixing on enhancing biomolecular processes in a microchannel flow was investigated considering both a stagnant fluid and a background fluid flow. The mechanical mixing was achieved by an oscillating flap. A detailed mathematical model was developed for solving the fluid flow equations, in conjunction with the employment of a distance function to represent the position of the moving flap. Scaling of the governing equations demonstrated that four dimensionless parameters, namely *Pe*, *Da*, κ_A, and the concentration ratio ε characterize the macromolecular motion. An order of magnitude analysis was conducted using realistic flow properties and surface reaction variables. The magnitudes of the three time scales, the diffusion time, reaction time, and residence time, governing the driving forces behind macromolecular motion, were also considered in the analysis.

The results of the numerical study show that the rates of biomolecular processes in a microchannel can be enhanced through the use of mechanical mixing. The magnitude of the positive effect on enhancing the reaction rates using mechanical mixing depends upon the given flow conditions, the placement of the reaction site, and the position of the moving mechanical flap. For flow in a microchannel, the optimal location for the moving flap is on the top wall. Under these flow conditions, the moving flap increases the surface wall concentration by 51% after 7.5 oscillations at a distance of $1/3L_f$ to the right of the flap. The moving flap behaves as a micropump moving the fluid with higher concentrations towards the reaction sites faster during the initial time period. As time progresses, the effect of the flap decreases and approaches a quasi-steady state value. For the case without background flow, the optimal location for the moving flap is on the bottom surface where the reaction occurs. Under these initial conditions, the moving flap increases the surface concentration by 16.3% after 7.5 oscillations at a distance of $2/3L_f$ to the right of the flap. In a stagnant fluid, the moving flap behaves as a stirring agent, bringing fluid with higher concentration towards the wall as the species are depleted in the concentration boundary layer. As the reaction proceeds, the rate of macromolecular removal increases with aiding effects from the oscillating flap. The results presented in this study can be used by experimentalists in the design and placement of reaction probes at optimal locations in a microdevice with a moving mechanical actuator.

Acknowledgements

This research was funded by the Indo–US Forum Joint Centre on Advanced and Futuristic Manufacturing and NSF US–India program Grant No. OISE-0526649. A special thanks to Tamal Das at the Biotechonology Department at IIT Kharagpur for sharing his knowledge on the DNA hybridization process.

References

[1] M.J. Madou, Fundamentals of Microfabrication: The Science of Miniaturization, CRC Press, Boca Raton, Florida, 2002.
[2] T. Gervais, K.F. Jensen, Mass transport and surface reactions in microfluidic systems, Chem. Eng. Sci. 61 (2006) 1102–1121.
[3] J. Kleimann, G. Lecoultre, G. Papastavrou, S. Jeanneret, P. Galleto, J.M. Koper, M. Borkovec, Deposition of nanosized latex particles onto silica and cellulose surfaces studied by optical reflectometry, J. Colloid Interface Sci. 303 (2006) 460–471.

[4] J.M. MacInnes, Computation of reacting electrokinetic flow in microchannel geometries, Chem. Eng. Sci. 57 (2002) 4539–4558.
[5] E.K. Zholkovskij, J.H. Masliyah, Hydrodynamic dispersion due to combined pressure-driven and electroosmotic flow through microchannels with a thin double layer, Anal. Chem. 76 (2004) 2708–2718.
[6] S. Das, T. Das, S. Chakraborty, Modeling of coupled momentum, heat and solute transport during DNA hybridization in a microchannel in the presence of electro-osmotic effects and axial pressure gradients, Microfluid. Nanofluid. 2 (2006) 37–49.
[7] S. Das, S. Chakraborty, Augmentation of macromolecular adsorption rates through transverse electric fields generated across patterned walls of a microfluidic channel, J. Appl. Phys. 100 (2006) 014908 (1–8).
[8] A. Ajdari, Transverse electrokinetic and microfluidic effects in micropatterned channels: lubrication analysis for slab geometries, Phys. Rev. E 65 (2001) 016301.
[9] S. Das, S. Chakraborty, Transverse electrodes for improved DNA hybridization in microchannels, AIChE J. 53 (2007) 1086–1099.
[10] S. Ramirez-Garcia, D. Diamond, Biomimetic low power pumps based on soft actuators, Sens. Actuators A 135 (1) (2007) 229–235.
[11] T.P. Burg, S.R. Manalis, Suspended microchannel resonators for biomolecular detection, Appl. Phys. Lett. 83 (13) (2003) 2698–2700.
[12] M.B. Viani, T.E. Schaffer, A. Chand, M. Rief, H.E. Gaub, P.K. Hansma, Small cantilevers for force spectroscopy of single molecules, J. Appl. Phys. 86 (4) (1999) 2258–2262.
[13] K. Pappaert, G. Desmet, A dimensionless number analysis of the hybridization process in diffusion- and convection-driven DNA microarray systems, J. Biotechnol. 123 (2006) 381–396.
[14] M.R. Henry, P.W. Stevens, J. Sun, D.M. Kelso, Real-time measurements of DNA hybridization on microparticles with fluorescence resonance energy transfer, Anal. Biochem. 276 (1999) 204–214.
[15] S. Osher, R. Fedkiw, Level Set Methods and Dynamic Implicit Surfaces, Applied Mathematical Sciences, 153, Springer, New York, 2003, pp. 17–22.